PCCP

ROYAL SOCIETY OF CHEMISTRY

PAPER

Published on 14 October 2026
Licensed under CC-BY 4.0

Check for updates

Cite this: DOI: 10.1039/d6cp02307j

Tip–sample distance dependence of local work function in Kelvin probe force microscopy on Pb/Si(111) islands

Daniel Rothhardt, †[a] Thomas Späth, [b] Paul P. Schmidt, ‡[a] Ralf Metzler [a] and Regina Hoffmann-Vogel [a]

Received 18th June 2026,
Accepted 9th October 2026

DOI: 10.1039/d6cp02307j

rsc.li/pccp

To gain a better understanding of the Kelvin probe force microscopy (KPFM) method, it is important to obtain a quantitative understanding of the measured contact potential difference (CPD) values as a function of the tip–sample distance. This will allow a more complete quantitative understanding of the electronic properties and the forces acting on the tip. Here, we chose Pb islands on a Si(111) 7 × 7 surface, metallic islands on a semiconducting surface. Using a scanning force microscope in frequency modulation mode, we perform point bias-approach measurements at 120 K on Pb islands. We investigate how the CPD changes as a function of tip–sample distance and how the electrostatic force changes as a function of the applied bias between the tip and the sample. The measured distance-dependence of the CPD not only allows a connection between the point-of-view of atomic resolution KPFM and of the averaging effects of the body of the tip but also allows the investigation of the shape of charged objects on the surface.

1 Introduction

Kelvin probe force microscopy (KPFM) is a method to determine local variations in the electrostatic potential of surfaces and nanostructures.[1,2] In this scanning force microscopy (SFM)-based technique, the electrostatic forces measured between the tip and the sample are minimized by applying a voltage to compensate for the bias-dependent electrostatic interaction, and the compensation voltage gives the contact potential difference (CPD). The measurements can be performed as a function of the tip–sample distance and voltage.[3] Voltage differences as small as 3–30 mV can be measured with high precision using the Kelvin method.[4,5] The measured CPD is an effective quantity rather than a purely local surface property. The electrostatic interaction is long ranged and can include contributions from the surface below the tip apex, the surrounding sample area, the tip cone, and the cantilever.[6] This capacitive averaging complicates quantitative CPD measurements, especially on nanostructured samples with finite lateral dimensions.[7–9] The influence of the tip–sample distance on the signal has been discussed critically.[9,10] Additionally, the dependence of the CPD on island size has been investigated.[9]

Electrostatic forces are known to be strongly distance-dependent.[11,12] The decay length of a certain Fourier component present in the sample is its wavelength. This allows for atomic resolution for short-range electrostatic forces under ultra-high vacuum conditions.[13–18] At the same time, long-range capacitive forces remain present and can cause a distance-dependent CPD. The measured value should therefore be understood as an effective local CPD that contains both local electronic information and the electrostatic weighting of the tip–sample geometry.

Pb islands on Si(111) are a suitable model system to investigate electrostatic forces, because metal islands are combined with a semiconducting surface, and the electronic properties of the system are well-known.[19,20] Additionally, the system shows interesting electronic properties such as the quantum size effect. Electron confinement in the film-normal direction leads to thickness-dependent electronic properties and work-function oscillations.[5,21,22] KPFM measurements on individual Pb islands showed even–odd work-function oscillations as a function of island height, demonstrating that SFM/KPFM can access quantum-size effects close to equilibrium.[5] Later work showed that the apparent Pb island thickness has to be corrected by one atomic layer, which changes the assignment of the bilayer work-function oscillation for thin islands.[5]

[a] Institut für Physik und Astronomie, Universität Potsdam, Karl-Liebknecht-Str. 24-25, 14476 Potsdam, Germany. E-mail: hoffmannvogel@uni-potsdam.de
[b] Physikalisches Institut, Karlsruhe Institute of Technology (KIT), 76131 Karlsruhe, Germany
† Present address: Magnetic and Functional Thin Films Laboratory, Empa, Swiss Federal Laboratories for Materials Science and Technology, 8600 Dübendorf, Switzerland.
‡ Present address: Department of Physics, Friedrich-Alexander Universität Erlangen-Nürnberg, Erwin-Rommel-Strasse 1, Erlangen, Germany.

Here, we study the distance dependence of the CPD on Pb islands on Si(111) and on the wetting layer surrounding the islands. We show that the CPD has a different distance dependence on the metal compared to the wetting layer. The distance dependence is in accordance with the expected distance dependence known from the shape of the objects in the macroscopic world. As expected, an island viewed as a plane capacitor shows a constant CPD whereas line-like objects show a logarithmic distance dependence due to long-range contributions to the electrostatic tip–sample interaction.

2 Experimental methods

As a substrate, we use phosphorous doped n-type Si(111) with a resistivity of ρ = 7.5 Ω cm. By briefly heating several times to 1200 °C in our vacuum chamber with a base pressure of 3×10^{-10} mbar, we achieve a clean reconstructed Si(111) 7 × 7 surface. We use electron beam evaporation (Oxford Applied Research, equipped with an ion flux monitor) to deposit Pb with a flux of 10–25 nA onto the Si(111) 7 × 7 surface kept at T = 300 K. Immediately after the deposition, we transfer the substrate into the SFM (Omicron VT-AFM) which had been cooled to 120 K by liquid nitrogen.

We use Si cantilevers (Nanosensors, Neuchatel, Switzerland (type PPP-NCL or type SSS-NCL) with a longitudinal spring constant c_L of 45 N m^{-1}, a resonance frequency f_0 of 158 kHz and a tip radius smaller than 10 nm which were cleaned by Ar ion sputtering and subsequent heating to 150 °C. The SFM measurements are performed in dynamic frequency modulation mode with a constant amplitude of 5 nm using a Nanonis (Specs Switzerland) electronics instrument. In the dynamic mode, the oscillation amplitude of the tip is kept constant and the frequency shift is used as a measure for the tip–sample interaction. Kelvin probe force microscopy imaging is performed by applying an oscillating voltage between tip and sample with a typical frequency of 300 Hz and a typical amplitude A_{KPFM} of 1 V. The feedback loop is operated to minimize the component of the frequency shift oscillating at the same frequency by applying a suitable DC bias voltage to the tip. However, the bias voltage sign convention has been chosen in such a way that it represents negative charge on the Si by large KPFM values—the same sign convention as used previously in ref. 5.

We record the bias approach data with a self-written script. First, the feed-back loop controlling tip–sample distance is stopped and the tip is retracted. Then, the cantilever is approached step by step and, at each point, the frequency shift and current are measured against the bias. We obtain three three-dimensional datasets of the frequency shift from which we calculate the force partly using the method introduced by Baratoff[23] and partly by the Sader–Jarvis method[24] and extract distance-dependent bias frequency shift data. In addition, we use the frequency shift distance curve measurement tool implemented in Nanonis to determine the force as a function of distance above Pb-islands and the wetting layer.

From the 3D data, we fit parabolae to the bias frequency shift data and determine the maximum, *i.e.* the CPD, at each tip–sample distance.

3 Results and discussion

Fig. 1(a) shows a topographical overview of Pb islands grown on a Si(111) 7 × 7 surface. The islands are mostly extended along the terraces with step edges running from the lower left corner of the image to its upper right one. Only in some cases the islands grow over more than one terrace. The plane has been adjusted such that different heights of islands directly result in different values of the gray scale. Fig. 1(b) shows the simultaneously recorded KPFM image. The Pb islands appear as dark regions and show a smaller CPD compared to the wetting layer. Among the islands, different CPD values in one island are resolved. We attribute these different values to the quantum size effect and to different numbers of monolayers (ML) in the same island due to ring structures in the topography and/or growth over several terraces.[5] The wetting layer shows a strongly inhomogeneous CPD due to its disordered nature and can show several phases which are also disordered. It is one atomic layer thick but contains more Pb (1.3 atomic layers) than one atomic layer of Pb. In previous publications island-shaped features on the wetting layer were attributed to the disappearance of islands as a function of time due to diffusion.[25] Here, we suppress such diffusion effects by transferring the substrate into the pre-cooled SFM directly after evaporation and conserve the wetting layer in its disordered state formed at the substrate temperature during deposition at 300 K by rapid cooling to liquid nitrogen temperatures.

Fig. 2(a) displays the frequency shift $\Delta f(V)$ measured with a different tip above a 5 ML high island (gray) and the wetting layer (red) as a function of voltage V. We describe the electrostatic force $F_{el}(z)$ by describing the tip and sample as a capacitor,

$$F_{el}(z) = \frac{1}{2}\frac{\partial C}{\partial z}(V - V_{CPD})^2 \quad (1)$$

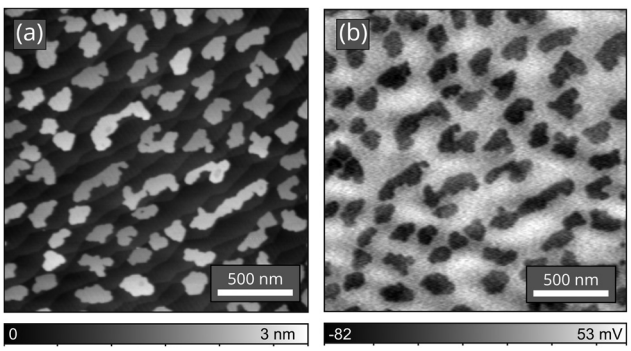


Fig. 1 (a) SFM topographic overview image of Pb islands with different numbers of monolayers (MLs). The wetting layer is located between the islands. (b) Corresponding KPFM measurement with CPD ranging from 82 mV to 53 mV. Frequency shift $\Delta f = -21$ Hz, cantilever oscillation amplitude A = 5 nm, spring constant c_L = 45 N m^{-1}, resonance frequency f_0 = 158 kHz, Kelvin frequency f_{KPFM} = 300 Hz, and Kelvin amplitude A_{KPFM} = 780 mV.

This journal is © the Owner Societies 2026

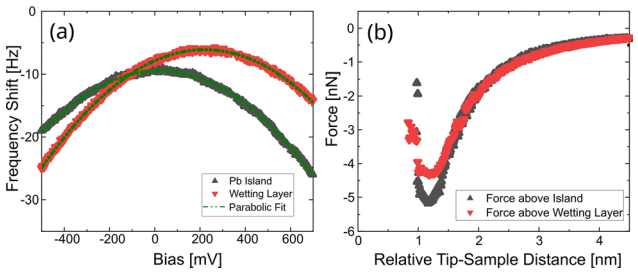


Fig. 2 (a) Frequency shift $\Delta f(V)$ curves show a parabolic dependence on the bias voltage, as expected. A parabolic fit is shown as two green dotted lines. The CPD amounts to about 220 mV between the wetting layer (red) and the Pb island (gray). (b) The force obtained as a function of tip–sample distance from the measured Δf data as described in the text shows a stronger contribution of attractive forces above the Pb island (gray) compared to the wetting layer (red) which lead to a down shift of the force minimum of about 0.8 nN. Cantilever oscillation amplitude A = 5 nm, spring constant c_L = 41 N m^{-1}, resonance frequency f_0 = 158 kHz, Kelvin frequency f_{KPFM} = 1000 Hz, and Kelvin amplitude A_{KPFM} = 500 mV.

where z is the tip–sample distance, C is the tip–sample capacitance and V_{CPD} is the contact potential difference measured in V. Often the tip is modelled as a cone with a spherical cap, where the part attributed to the sphere against a metallic surface is given by

$$F_{el}(z) = \pi\varepsilon_0(V - V_{CPD})^2 \frac{{R_{tip}}^2(1-\sin\theta_0)}{z\left[z + R_{tip}(1-\sin\theta_0)\right]}. \qquad (2)$$

Here, ε_0 is the vacuum permittivity, R_{tip} is the radius of the spherical part of the tip, and θ_0 is the tip opening angle.[26,27] The acquired spectra were fitted with a parabola as shown in green color. The maximum of the parabola corresponds to the CPD between the tip and the surface. Determining the maxima of both curves reveals a CPD of 300 mV between a Pb island and the wetting layer measured with a different tip. The CPD of the island is lower than that of the wetting layer as expected from the KPFM measurements, shown in Fig. 1(b).

Both the SFM (Fig. 1(a)) and the $\Delta f(V)$ (Fig. 2(a)) measurements suggest stronger attractive forces, *i.e.* a larger negative frequency shift at V_{CPD}, above the Pb islands compared to the wetting layer. To study the tip–sample interaction in more detail, we measure the frequency shift as a function of distance above an island and the wetting layer. In Fig. 2(b) we show the calculated force obtained from the $\Delta f(z)$ measurement. During the measurement of $\Delta f(z)$, we compensate the electrostatic force by applying the constant CPD determined at a given large tip–sample distance to the tip for both the Pb island and the wetting layer respectively. We observe almost no differences between the island and the wetting layer at large tip–sample distances. Near the point of closest approach to the surface, the force minimum is shifted towards lower force values by approx. 0.8 nN over the Pb island compared to the wetting layer. We attribute this shift to stronger attractive forces, to a stronger chemical tip–sample interaction, and/or to stronger electrostatic attractive forces above the wetting layer compared to the Pb island.

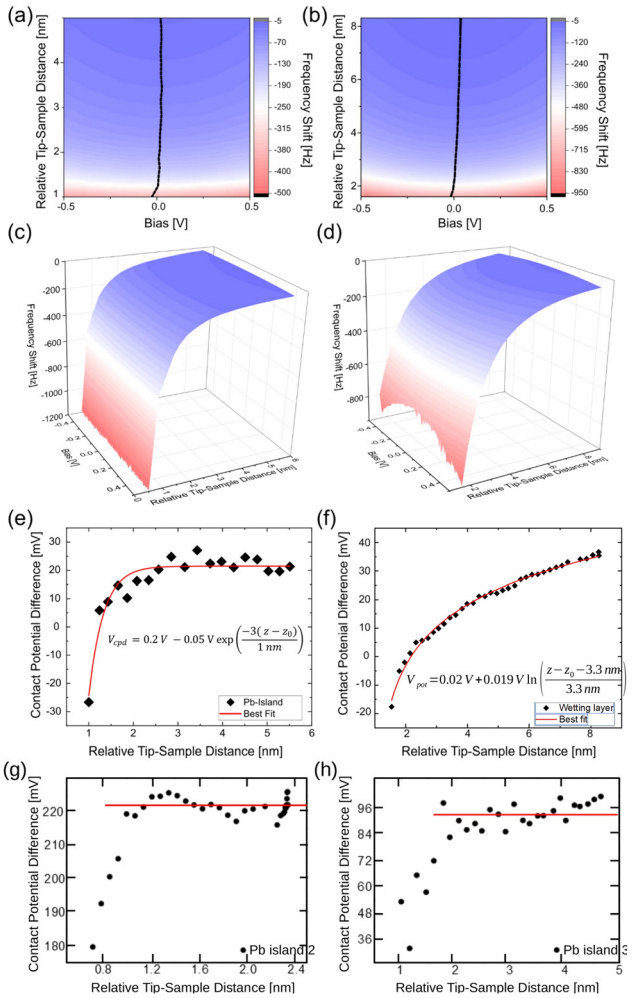


Fig. 3 $\Delta f(V, z)$ data obtained over a 6 ML high island (a) and over the wetting layer (b). The voltage is shown on the x-axis and the tip–sample distance z is shown on the y-axis, while the frequency shift is color-coded. The black line marks the CPD as a function of distance. (c) and (d) 3D representation of (a) and (b). (e) and (f) Distance dependence of the CPD for a Pb island (e) and the wetting layer (f) obtained from the data shown in (a) and (b). The data in part (e) is well-described by an exponential function shown in red as a guide to the eye. The values of the function are given in the inset of the figure. (g) and (h) Data obtained on additional islands.

In order to study the electrostatic potential in more detail, we perform $\Delta f(V, z)$ measurements on the same island and the same area on the wetting layer. Fig. 3 shows the frequency shift (a) for the Pb island and in (b) above the wetting layer as a function of both tip–sample distance and bias voltage. At all distances the bias-dependence of the data is well-described by a parabolic fit function. We determine the CPD values by fitting such a parabola to each curve. The result is shown in black in Fig. 3(a) for the Pb island and (b) for the wetting layer. Panel (c) and (d) show the same data in a three-dimensional parametric representation. We clearly observe a parabolic dependence of the force on the voltage even at the closest tip–sample distances for the wetting layer. In panels (e) and (f) we present the CPD values obtained by the parabolic fit as a function of the tip–sample distance, the same data as the black line in Fig. 3(a) and (b).

While the CPD of the wetting layer (Fig. 3(f)) shows a clear long-range distance-dependence, *i.e.* a variation above 1–2 nm distance, the CPD of the island (Fig. 3(e)) shows a steep increase at short tip–sample distances and then remains roughly constant. Also the measurement taken above two additional islands shows a strong increase followed by a constant (Fig. 3(g) and (h)).

We first discuss the steep increase in the short-range regime in terms of either chemical bonding, which can result in charge transfer and can generally be regarded as of electrostatic origin, or the distance-dependence of electrostatic forces viewed from classic electrostatics. To evaluate the tip–sample distance at which it is relevant, it is important to describe how the tip–sample distance has been calibrated: here, we use the tunneling current I_T to calibrate the tip–sample distance z, *i.e.* we measure $I_T(z)$ data and set the z-value of the I_T onset to $z = 1$ nm.

We expect that these chemical bonds have a range of the tunneling distance, approximately 1 nm. Also, we expect atomic-scale electrostatic forces to be relevant at the same distances. The atomic-scale arrangement itself has a two-dimensional periodicity of wavelength λ, and this leads to electrostatic Fourier components of the decay length λ as is well-known from textbooks and has also been observed in previous experimental studies.[28,29] Here, we use the 2d Fourier transform, where the x-axis and the y axis of a function are Fourier-transformed, whereas the z-axis is left unchanged and solve the Laplace equation in the space above the sample. In general, we expect an exponential decay of the electrostatic field 2d Fourier components of the potential Φ where the decay constant λ is the lateral wavelength of the respective 2d Fourier component,[28] *i.e.*

$$\Phi(z) = A_0 \exp(-(z - z_0)/\lambda) + \Phi_0. \quad (3)$$

Here, A_0 and z_0 are parameters to adjust the tip–sample distance one of which is redundant, and Φ_0 allows adjustment for a different choice of the zero level for voltages.

In Fig. 3(e), a decay constant λ of about 1/3 nm is not in contradiction to a suitable description of the distance-dependence observed in the experiment, a value close to interatomic distances. This agrees well with the findings in ref. 30, where a Si(111) 7 × 7 was investigated experimentally as well as by simulations. However, the distance dependence varies from sample to sample. As shown in Fig. 3(g), the data are compatible with a decay length of approximately 0.4 nm and as shown in Fig. 3(h) with a decay length of approximately 1 nm. In any case, only the tip apex is affected by these forces; hence, there is no tip-averaging effect in this case due to the short-range nature of the forces. Additionally atomic relaxation could lead to altering the functional dependence of the force on tip–sample distance.

We compare these results to the measurements of KBr islands on InSb(001),[9] where an insulator on a semiconductor surface was studied. Also in this case a clear CPD change was observed on the islands compared to the bare surface due to uncompensated charge in the island. The distance-dependence there was also on the order of 1 nm, but somewhat larger as compared to our value, possibly due to differences in the short-range chemical forces and/or electrostatic forces above KBr (in ref. 9) as compared to Pb (here). Since the decay length of the CPD change is somewhat larger and the measurement distance range is shorter, it is less clearly observed that the CPD becomes constant at large tip–sample distances as expected for an object resembling a plane capacitor of infinite lateral size.

Next, we turn to the data obtained above the wetting layer (Fig. 3(f)). The data look surprisingly similar to the ones obtained recently above a graphene nanoribbon on the Au(111) surface:[31] Apart from a shift of the absolute values of the CPD, and a recalibration of the z-scale of approximately a factor of 10, the data appear similar in Fig. 3(f) compared to the data shown in ref. 31. For the graphene nanoribbon, the CPD *versus* distance data were described by a logarithmic dependence, related to a one-dimensional model of a line charge, a cylindrical capacitor:

$$\Phi(z) = \frac{\rho}{2\pi\varepsilon_0} \ln\left(\frac{z - R_{\mathrm{circcap}}}{R_{\mathrm{circcap}}}\right) + \Phi_0 \quad (4)$$

where ρ is the charge per unit length. For this ln-function, there is a parameter R_{circcap} that adjusts the radius of the circular capacitor. The radius of the circular capacitor R_{circcap} leads to a sharper function with stronger changes if the radius is smaller and to a more smoothly varying function if the radius is larger. By fitting, we obtain for the radius R_{circcap} the value 3.3 nm. The comparison between the data shown here and the ones from ref. 31 leads us to conclude that the object causing the distance dependence shown here is about three times larger in size compared to the width of a graphene nanoribbon, of approximately 1 nm width. The line charge is obtained to be approximately 7×10^{-3}e nm^{-1}, a weak charge.

This points to the fact that the electrostatics of the wetting layer can be modelled by one or more line-like objects. In order to identify which objects could be causing these electrostatic forces, one could think about the Pb on Si itself, about domain boundaries of differently ordered phases, line-like phases, step edges or the edges of Pb islands. We assess that the edges of the Pb islands are likely to be too far away from a central position on the wetting layer, given the structure shown in Fig. 1. The step edges[18] are located below the islands as well as the wetting layer, but apparently do not influence the island KPFM measurement possibly due to the shielding by the metallic overlayer. The shielding of the wetting layer could be insufficient or the charge of the step edges in this region could differ from the ones located below the island. Additionally, Pb on Si(111) shows phases that form line-like objects, *e.g.* the incommensurate striped phase.[32–34]

We now turn to the influence of the tip on the measurement. In what has been discussed above, a possible influence of the tip, leading to averaging over a large area of the surface, has not been detected although we expect that it must exist. Also for the graphene nanoribbons (ref. 31), it turned out to be unnecessary to include the shape of the tip in the considerations. Also there the CPD had been compensated by applying a voltage between the tip and the sample during imaging. Only static charge distributions that are not compensated by applying a voltage could lead to measurable forces. These static charge distributions have the shape of the sample capacitor and are mimicked in the tip (or *vice versa*). We can summarize that for many

 This journal is © the Owner Societies 2026

nanostructures, the same laws apply as in the macroscopic world and that, indeed, in many cases, the tip can be thought of as a perfect metal that mimics the sample charge distribution given by its shape. Only if the relevant Fourier components of the tip and the sample and the distance range studied are of the same order, a more complicated analysis is necessary.

4 Conclusions

We studied the CPD as a function of the tip–sample distance for Pb islands on a Si(111) 7 × 7 surface and on the wetting layer. While the CPD on the island showed a short-range dependence of the atomic scale followed by a constant regime with no dependence on distance, the data on the wetting layer demonstrated a strong distance-dependence that we relate to local line-like inhomogeneities at the scale of less than about 10 nm. For the island, the tip is well-described by a perfect metal that mimics the charge distribution of the sample. Our results are the basis for the investigation of time-dependent electrostatic forces, both studied in a quasi-static way[35] and for increasingly short time-scales.

Author contributions

Daniel Rothhardt: investigation and writing – original draft. Thomas Späth: investigation. Paul P. Schmidt: investigation. Ralf Metzler: supervision, writing – review and editing. Regina Hoffmann-Vogel: methodology, resources, supervision and writing – review and editing.

Conflicts of interest

There are no conflicts to declare.

Data availability

The data are publicly available at Zenodo at DOI: https://doi.org/10.5281/zenodo.20142345.

Acknowledgements

We acknowledge enlightening discussion with Hans Hug, Felix Hartmann, Janet Anders, Zeineb Ben Tanfous, Gino Wegner and Kurt Busch, as well as help with programming by Manuel Schulze and funding from the German Science Foundation (DFG Grants No. 513075417 and 318763901).

Notes and references

1 J. M. R. Weaver and D. W. Abraham, *J. Vac. Sci. Technol., B*, 1991, **9**, 1559.
2 M. Nonnenmacher, M. P. Oboyle and H. K. Wickramasinghe, *Appl. Phys. Lett.*, 1991, **58**, 2921.
3 L. Collins, M. B. Okatan, Q. Li, I. I. Kravenchenko, N. V. Lavrik, S. V. Kalinin, B. J. Rodriguez and S. Jesse, *Nanotechnology*, 2015, **26**, 175707.
4 P. P. Schmidt, F. Hartmann, L. Faber, R. Metzler, J. Anders and R. Hoffmann-Vogel, *Phys. Rev. B*, 2024, **110**, 235422.
5 T. Späth, M. Popp, C. P. León, M. Marz and R. Hoffmann-Vogel, *Nanoscale*, 2017, **9**, 7868.
6 Z. M. Ma, L. Kou, Y. Naitoh, Y. J. Li and Y. Sugawara, *Nanotechnology*, 2013, **24**, 225701.
7 T. Shiota and K. Nakayama, *Jpn. J. Appl. Phys.*, 2001, **40**, L986.
8 S. Sadewasser and M. C. Lux-Steiner, *Phys. Rev. Lett.*, 2003, **91**, 266101.
9 F. Krok, K. Sajewicz, J. Konior, M. Goryl, P. Piatkowski and M. Szymonski, *Phys. Rev. B:Condens. Matter Mater. Phys.*, 2008, **77**, 235427.
10 L. Nony, F. Bocquet, C. Loppacher and T. Glatzel, *Nanotechnology*, 2009, **20**, 264014.
11 S. Hudlet, M. S. Jean, C. Guthmann and J. Berger, *Eur. Phys. J. B*, 1998, **2**, 5.
12 R. Hoffmann, M. A. Lantz, H. J. Hug, P. J. A. van Schendel, P. Kappenberger, S. Martin, A. Baratoff and H.-J. Güntherodt, *Phys. Rev. B:Condens. Matter Mater. Phys.*, 2003, **67**, 085402.
13 S. Kitamura, K. Suzuki, M. Iwatsuki and C. B. Mooney, *Appl. Surf. Sci.*, 2000, **157**, 222.
14 K. Okamoto, Y. Sugawara and S. Morita, *Appl. Surf. Sci.*, 2000, **188**, 381.
15 G. H. Enevoldsen, T. Glatzel, M. C. Christensen, J. V. Lauritsen and F. Besenbacher, *Phys. Rev. Lett.*, 2008, **100**, 236104.
16 S. Sadewasser, P. Jelinek, C.-K. Fang, O. Custance, Y. Yamada, Y. Sugimoto, M. Abe and S. Morita, *Phys. Rev. Lett.*, 2009, **103**, 266103.
17 L. Gross, F. Mohn, P. Liljeroth, J. Repp, F. J. Giessibl and G. Meyer, *Science*, 2009, **324**, 1429.
18 C. Pérez León, H. Drees, S. Wippermann, M. Marz and R. Hoffmann-Vogel, *J. Phys. Chem. Lett.*, 2016, **7**, 426.
19 I. B. Altfeder, K. A. Matveev and D. M. Chen, *Phys. Rev. Lett.*, 1997, **78**, 2815.
20 Y. Han, J. Zhu, F. Liu, S.-C. Li, J.-F. Jia, Y.-F. Zhang and Q.-K. Xue, *Phys. Rev. Lett.*, 2004, **93**, 106102.
21 V. Yeh, L. Berbil-Bautista, C. Z. Wang, K. M. Ho and M. C. Tringides, *Phys. Rev. Lett.*, 2000, **85**, 5158.
22 W. B. Su, S. H. Chang, W. B. Jian, C. S. Chang, L. J. Chen and T. T. Tsong, *Phys. Rev. Lett.*, 2001, **86**, 5116.
23 O. Pfeiffer, R. Bennewitz, A. Baratoff, E. Meyer and P. Grutter, *Phys. Rev. B:Condens. Matter Mater. Phys.*, 2002, **125**, 161403.
24 J. E. Sader and S. P. Jarvis, *Appl. Phys. Lett.*, 2004, **84**, 1801.
25 T. Späth, M. Popp and R. Hoffmann-Vogel, *Phys. Rev. Lett.*, 2020, **124**, 016101.
26 M. Saint Jean, S. Hudlet, C. Guthmann and J. Berger, *J. Appl. Phys.*, 1999, **86**, 5245.
27 S. Hudlet, M. Saint Jean, B. Roulet, J. Berger and C. Guthmann, *J. Appl. Phys.*, 1995, **77**, 3308.

28 R. P. Feynman, R. B. Leighton and M. Sands, *The Feynman Lectures on Physics II*, Addison-Wesley Publishing Group, Reading, Massachusets, 1964.
29 M. A. Lantz, H. J. Hug, R. Hoffmann, S. Martin, A. Baratoff and H.-J. Güntherodt, *Phys. Rev. B:Condens. Matter Mater. Phys.*, 2003, **68**, 035324.
30 S. Kawai, T. Glatzel, H. J. Hug and E. Meyer, *Nanotechnology*, 2010, **21**, 245704.
31 D. Rothhardt, A. Kimouche, T. Klamroth and R. Hoffmann-Vogel, *Beilstein J. Nanotechnol.*, 2024, **15**, 1125.
32 M. Yakes, V. Yeh, M. Hupalo and M. C. Tringides, *Phys. Rev. B:Condens. Matter Mater. Phys.*, 2004, **69**, 224103.
33 S. Stepanovsky, M. Yakes, V. Yeh, M. Hupalo and M. C. Tringides, *Surf. Sci.*, 2006, **600**, 1417.
34 J. S. M. Hupalo and M. C. Tringides, *Phys. Rev. Lett.*, 2003, **90**, 216106.
35 M. Navarro-Rodriguez, P. P. Schmidt, R. Hoffmann-Vogel, A. M. Somoza and E. Palacios-Lidon, *Phys. Rev. B*, 2025, **112**, 085419.

 This journal is © the Owner Societies 2026